

# Quantum scattering model of energy transfer in photosynthetic complexes

Bao-quan Ai<sup>1</sup> and Shi-Liang Zhu<sup>1,2\*</sup>

<sup>1</sup>Laboratory of Quantum Information Technology and SPTE,  
South China Normal University, Guangzhou, China

<sup>2</sup> Center for Quantum Information, IIS, Tsinghua University

We develop a quantum scattering model to describe the exciton transport through the Fenna-Matthews-Olson (FMO) complex. It is found that the exciton transport involved the optimal quantum coherence is more efficient than that involved classical behavior alone. Furthermore, we also find that the quantum resonance condition is easier to be fulfilled in multiple pathways than that in one pathway. We then definitely demonstrate that the optimal distribution of the pigments, the multitude of energy delivery pathways and the quantum effects, are combined together to contribute to the perfect energy transport in the FMO complex.

PACS numbers: 87.15.A-; 71.35.-y; 87.15. hj

Photosynthesis is a fundamental biological process that harvests solar energy to power life on Earth. It starts with the absorption of a photon of sunlight by the antenna molecules, followed by transfer of the energy to the reaction centers. Remarkably, the energy transfer from the antennas to the reaction center is almost perfectly efficient[1]. Then an intriguing question arises: what makes the energy transfer so efficient? Up to date, there are two acceptable contributing factors[2]: The first one is optimal space distribution of the pigments in light-harvesting complexes[3], where the optimal space is just closely enough to enable fast energy transfer, but far enough apart to prevent the molecular orbital of the pigments from overlapping. The second factor is the supramolecular organization of photosynthetic apparatus, which allows the multiple energy delivery pathways to connect to the reaction centre[4].

Recently, the experimental and theoretical studies show that there exists long-lived quantum coherence in this energy transfer in several photosynthetic complexes [5–10], which suggests that quantum coherence could be a third factor in optimizing energy transfer efficiency. However, to what extent quantum effects contribute to the efficiency of energy transfer is largely unknown. Therefore, it would be significant important to establish quantitatively whether or not photosynthetic light harvesting that involves quantum coherence is truly more efficient than it would be using classical mechanisms alone[2].

In this paper, we develop a quantum scattering model to describe the exciton (the energy carrier) transport in the FMO complex. We explore respectively the quantum and classical transports of the exciton in one, two and multiple pathways and show that the quantum transport under the resonant condition can lead to perfect efficiency. Since the resonance is due to the quantum coherence and it is impossible in classical physics, we thus demonstrate definitely that the exciton transport involved optimal quantum coherence is more efficient than that for the classical case. We show that the resonant transport with perfect efficiency occurs when the quan-

tum phase of the exciton accumulated in the pathways are fulfilled with the resonant condition. Since the phase of the exciton is determined by the space distribution of the pigments, the optimal distribution of the pigments is then indeed significant in the near-unity transfer efficiency. Although the perfect efficiency is also possible for one pathway alone, the multiple pathways are essential because the resonant region in multiple pathways is much larger than that in one pathway. The large resonant region is the mechanism that the excitons with a broad range of the spectrum ( electron absorbed different colors of light) can transport with perfect efficiency. Therefore, the three mentioned contributing factors, the optimal distribution of the pigments, the multitude of energy delivery pathways and the quantum effects, are combined together in our proposed model to contribute the perfect energy transport in FMO.

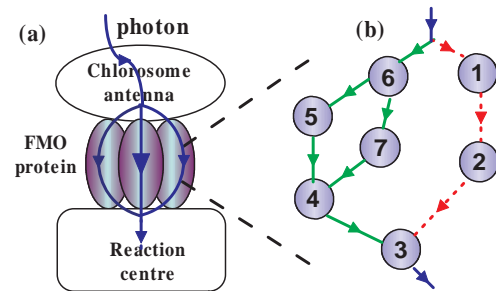


FIG. 1. (Color online) The schematic representation of the light-harvesting apparatus of green sulphur bacteria. (a) The light is absorbed by the chlorosome antenna and then transported to the reaction center through the FMO complex. (b) Each monomer has seven pigments labelled by ① – ⑦. Two main energy transfer pathways  $L_A$  and  $L_B$  are indicated by the red and green arrows [11],  $L_A$ : ①→②→③;  $L_B$ : a ring structure contains two paths ⑥→⑤→④→③ and ⑥→⑦→④→③.

*Quantum scattering model of the FMO complex.* The architecture of antenna light-harvesting complexes varies widely among photosynthetic organisms. A well-studied

example is the water-soluble FMO complex of green sulfur bacteria. As shown in Fig. 1, the FMO complex comprises three identical monomers that each contains seven pigments. The seven pigments (Fig. 1(b)) can be combined into two major energy transport pathways [11]. A light pulse absorbed by the chlorosome antenna could excite an electron into a state called an exciton which is a quasi-particle and can be considered as the energy carrier in light-harvesting complexes. The exciton then transports to the reaction centre through FMO with nearly perfect efficiency.

Exciton transport is accomplished in FMO through tunneling, where the exciton jumps from one pigment to another. In the previous theories[9, 10, 12], each pigment is usually modeled by a two-level molecule and then the FMO complex are described by some coupled two-level molecules interacting with their environmental phonons. In this paper we proposed a different model, the scattering model[13, 14] (see a brief review in Supplementary material), to explain transmission efficiency of FMO. There are two basic elements in the scattering model, the scatterer and the ideal channel; they are connected with certain orders to form a quantum network. We denote the transfer matrix for the  $n$ th scatterer as  $M_n$  and the transfer matrix for the ideal channel with the length  $l$  as  $U_l$ . They can be written as

$$M_n = \begin{pmatrix} \frac{1}{t_n^*} & -\frac{r_n^*}{t_n^*} \\ -\frac{r_n}{t_n} & \frac{1}{t_n} \end{pmatrix}, \quad U_l = \begin{pmatrix} e^{-ikl} & 0 \\ 0 & e^{ikl} \end{pmatrix}, \quad (1)$$

where  $t_n = T_n^{\frac{1}{2}} e^{i\varphi_n}$ ,  $r_n = -iR_n^{\frac{1}{2}} e^{i\varphi_n}$ ,  $T_n$  is the transmission probability of the  $n$ th scatterer,  $R_n = 1 - T_n$  is its reflection probability,  $\varphi_n$  is the phase change in the transmitted wave and  $k$  is the wave number of the exciton.

The transport of FMO can be well explored with the help of the transfer matrices in Eq. (1) as well as the junctions  $S$  and  $G$  to be defined below. Each pigment can be thought of as a potential well and there exists a potential barrier between two nearest neighbor pigments along the pathways. The potential barrier can be well described by the transfer matrix of the scatterer defined in Eq.(1). The wave function of the exciton in pigment  $j$  could be written as  $\psi_j(x) = C_j e^{ikx} + D_j e^{-ikx}$ , where  $C_j$  and  $D_j$  are the amplitudes of the wave function. The amplitudes  $C_j$  and  $D_j$  are related to its nearest neighbor pigment through the transfer matrix of the scatterer between the two pigments. In addition, the transfer matrix of the pigment is the one as the ideal channel defined in Eq.(1). Therefore, we can describe the exciton transmission through the whole FMO complex with the following three steps: (i) the two major energy transport pathways in each monomer is described by two different scattering pathways  $L_A$  and  $L_B$ , as shown in Fig. 2(a). (ii) Each monomer is represented by a ring with two branches  $L_A$  and  $L_B$  and connected to two leads through two junctions  $S$ . The transfer matrix of the monomer  $j$  ( $j=1, 2, 3$ ) is

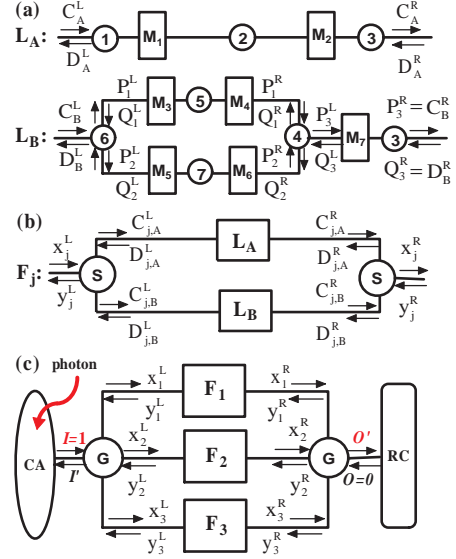


FIG. 2. The quantum scattering model we proposed to describe the excitation transmission of FMO. (a) The scattering matrix representation of two major pathways  $L_A$  and  $L_B$ . (b) Each monomer is represented by the symbol  $F_j$  made by a ring with two branches  $L_A$  and  $L_B$  and connected to two leads. (c) The scattering matrix representation of the whole FMO complex. The symbols near the arrows denote the corresponding transmitted and reflected amplitudes.

denoted as  $F_j$ , as show in Fig. 2(b). (iii) The transport of the whole FMO can be described in Fig. 2(c), where three monomers represented by  $F_j$  are connected to the antennas and reaction center through two junctions  $G$ . The exciton created at the antennas injects into FMO with  $I = 1$  through the  $G$  junction connected with the antennas. For simplicity, we assume that there is no reflection from the reaction center (the amplitude  $O$  in Fig. 2(c) vanishes); In this case, the transmission coefficient of the whole FMO complex is then determined by the probability  $|O'^2|$  indicated in Fig. 2(c).

*Transfer matrices of the FMO complex.* We now turn to study the transfer matrices of the basic elements  $L_A$ ,  $L_B$ ,  $F_j$  and the whole FMO complex. The pathway  $L_A$  is represented by two scatterers connected one ideal channel and its transfer matrix is then given by

$$L_A = M_2 U_l M_1, \quad (2)$$

where  $l$  is the length of the 2nd pigment. The pathway  $L_B$  is composed of three branches connected by two  $S$  junctions (⑥ and ④). For each branch, we have

$$\begin{pmatrix} P_m^R \\ Q_m^R \end{pmatrix} = \Gamma_m \begin{pmatrix} P_m^L \\ Q_m^L \end{pmatrix}, \quad (m = 1, 2, 3) \quad (3)$$

where  $\Gamma_1 = U_{l_1} M_4 U_{l_1} M_3 U_{l_1}$ ,  $\Gamma_2 = U_{l_2} M_6 U_{l_2} M_5 U_{l_2}$  and  $\Gamma_3 = M_7 U_{l_3}$ . Here  $l_m$  is the distance between the scatterers or the distance between the scatterers and the junctions for the  $m$ th branch. The amplitudes of the three

outgoing waves of the junction  $S$  are related by a  $S$  matrix to the amplitudes of the three incoming waves, i.e.,

$$\begin{pmatrix} D_B^L \\ P_1^L \\ P_2^L \end{pmatrix} = S \begin{pmatrix} C_B^L \\ Q_1^L \\ Q_2^L \end{pmatrix}, \quad \begin{pmatrix} P_3^L \\ Q_1^R \\ Q_2^R \end{pmatrix} = S \begin{pmatrix} Q_3^L \\ P_1^R \\ P_2^R \end{pmatrix}, \quad (4)$$

where  $S$  is a  $3 \times 3$  unitary matrix and its detailed form is given by Eq. (14) in Supplementary material.

From Eqs. (1-4), the amplitudes  $C_\alpha^L, D_\alpha^L$  ( $\alpha=A, B$ ) of the wave function on the left of the pathway and the amplitudes  $C_\alpha^R, D_\alpha^R$  on the right of the pathway can be related by the transfer matrixes  $L_\alpha$ , that is,

$$\begin{pmatrix} C_\alpha^R \\ D_\alpha^R \end{pmatrix} = L_\alpha \begin{pmatrix} C_\alpha^L \\ D_\alpha^L \end{pmatrix}. \quad (5)$$

Therefore, instead of an array of the scatterers, each pathway may be replaced by an effective transfer matrix.

We now study the exciton transport in one monomer of the trimer. The schematic representation of the monomer is shown in Fig. 2(b). Two pathways  $L_A$  and  $L_B$  form a ring and connected to two leads through two  $S$  junctions. With the help of the effective transfer matrix for the pathway  $\alpha$  of the monomer  $j$ , we can obtain

$$\begin{pmatrix} C_{j,\alpha}^R \\ D_{j,\alpha}^R \end{pmatrix} = L_{j,\alpha} \begin{pmatrix} C_{j,\alpha}^L \\ D_{j,\alpha}^L \end{pmatrix}, \quad (j = 1, 2, 3) \quad (6)$$

where  $L_{j,\alpha} = U_{l_{j,\alpha}} M_{j,\alpha} U_{l_{j,\alpha}}$ , and  $l_{j,\alpha}$  is the distance between the scatterers and  $S$  junctions for the pathway  $\alpha$  of the monomer  $j$ .

The amplitudes of the three outgoing waves are related to the amplitudes of the three incoming waves through  $S$  matrix given by

$$\begin{pmatrix} y_j^L \\ C_{j,A}^L \\ C_{j,B}^L \end{pmatrix} = S \begin{pmatrix} x_j^L \\ D_{j,A}^L \\ D_{j,B}^L \end{pmatrix}, \quad \begin{pmatrix} x_j^R \\ D_{j,A}^R \\ D_{j,B}^R \end{pmatrix} = S \begin{pmatrix} y_j^R \\ C_{j,A}^R \\ C_{j,B}^R \end{pmatrix}. \quad (7)$$

From Eqs. (6-7), the amplitudes of the wave function on the left of the monomer  $j$  and the amplitudes on the right are related by the matrix  $F_j$  given by

$$\begin{pmatrix} x_j^R \\ y_j^R \end{pmatrix} = F_j \begin{pmatrix} x_j^L \\ y_j^L \end{pmatrix}. \quad (8)$$

Similar to the transmission of one monomer, we can describe the exciton transport through FMO by two  $G$  junctions as shown in Fig. 2 (c). The amplitudes of the four outgoing waves of the junction  $G$  are related by a  $G$  matrix to the amplitudes of the four incoming waves

$$\begin{pmatrix} I' \\ x_1^L \\ x_2^L \\ x_3^L \end{pmatrix} = G \begin{pmatrix} I \\ y_1^L \\ y_2^L \\ y_3^L \end{pmatrix}, \quad \begin{pmatrix} O' \\ y_1^R \\ y_2^R \\ y_3^R \end{pmatrix} = G \begin{pmatrix} O \\ x_1^R \\ x_2^R \\ x_3^R \end{pmatrix}, \quad (9)$$

where  $G$  is a  $4 \times 4$  unitary matrix given by Eq. (20) in Supplementary material. By solving Eq.(9) with  $I=1$

and  $O=0$ , one can obtain the transmission coefficient  $T_{FMO} = |O'^2|$  of the FMO complex.

To understand the features of the transmission, we compare the transmission coefficients for different number of pathways. For simplicity, we assume that all scatterers have the same transmission probability  $T_n=T$  and the phase change in transmitted wave  $\varphi_n=0$ . Furthermore, we compare the transmission difference between the classical and quantum cases. As for the classical transmission, it means that the exciton is a classical particle without wave-like phase and thus the particle probability is determined by the addition of the probability from different pathways and not the amplitudes of the wave function; In addition, the scatterer is determined uniquely by the transmission probability  $T$ .

*Transmission of the pathways  $L_A$  and  $L_B$ .* Based on Eqs. (1,2,5), we can obtain the total transmission probability  $T_A = |C_A^R|^2$  for pathway  $L_A$  under the conditions  $C_A^L=1$  and  $D_A^R=0$ ,

$$T_A = T^2 / [T^2 + 4(1-T) \cos^2 \phi_A], \quad (10)$$

where  $\phi_A = kl$ . It is notable that the resonant tunneling  $T_A=1$  appears under the condition  $\phi_A = (n + 1/2)\pi$  with  $n$  being an integer. However, as for the classical case, after considering the multi-reflection between the scatterers  $M_1$  and  $M_2$ , we may obtain the total transmission probability  $T_A^C = \frac{T}{2-T}$ .

Figure 3(a) shows the total transmission probability as a function of the path phase for both quantum and classical case at strong scattering limit  $T=0.01$ . For classical case,  $T_A^C = 5 \times 10^{-3}$ , it is impossible for the particle to pass through the system at strong scattering limit. However, for quantum case, there exist two resonant peaks at which the total transmission probability takes its maximal value  $T_A=1$ . Therefore, the transport involved optimal quantum coherence is more efficient than that involved the classical behaviors alone.

For pathway  $L_B$ , we set  $C_B^L=1$ ,  $D_B^R=0$ ,  $kl_1=kl_2=\phi_B$  and  $kl_3=\phi'_B$ . From Eqs. (2-5), the total transmission probability  $T_B = |C_B^R|^2$  is given by

$$T_B = \frac{T^3}{T^2 \sin^2 \gamma + [(1+R) \cos \gamma + 2R \cos \phi'_B]^2}, \quad (11)$$

where  $\gamma = 2\phi_B + \phi'_B$ . The resonant tunneling  $T_B=1$  will happen under the conditions  $\gamma=\pi$  and  $\phi_B = \frac{1}{2} \arcsin[(T^{\frac{3}{2}} + T - 2)/2R]$ .

The path phases  $\phi_A$ ,  $\phi_B$  and  $\phi'_B$  denote the distance between the neighbor scatterers or the distance between the scatterers and junctions, which are determined actually by the space distribution of the seven pigments. When the pigments are optimally spaced such that  $\phi_A = \frac{1}{2}\pi$  for  $L_A$  and  $\gamma=\pi$ ,  $\phi_B = \frac{1}{2} \arcsin[(T^{\frac{3}{2}} + T - 2)/2R]$  for  $L_B$ , the quantum resonant tunneling will happen and the exciton can pass through the barriers with perfect efficiency. Therefore, we have theoretically

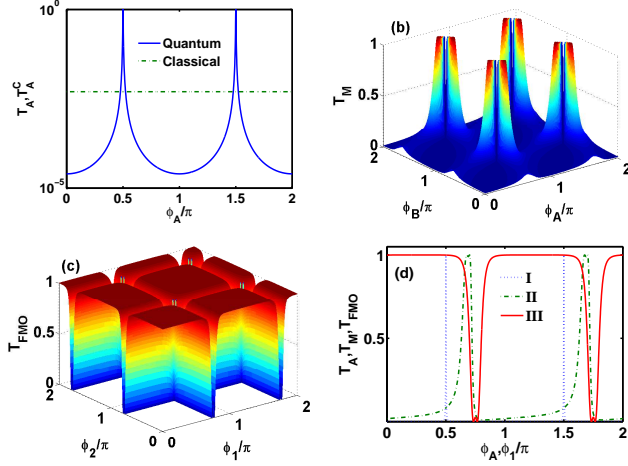


FIG. 3. (Color online) The transmission probability as a function of the path phases at  $T=0.01$ . (a) Single pathway  $L_A$  for both quantum and classical cases. (b) A monomer with double pathways. (c) The whole FMO with multiple pathways at  $\phi_3 = \frac{1}{2} \arcsin(\sqrt{0.12T} - \sqrt{R})$ . (d) The resonant structures: (I) one pathway  $L_A$ , (II) two pathways at  $\phi_B = \frac{1}{2} \arcsin(\sqrt{T} - \sqrt{R})$ , (III) multiple pathways at  $\phi_1 + \phi_2 = \pi/2$  and  $\phi_3 = \frac{1}{2} \arcsin(\sqrt{0.12T} - \sqrt{R})$ .

demonstrated that optimally spaced pigments in light-harvesting complexes can facilitate the energy transfer.

*Transmission of one monomer.* From Eqs. (6-8), we can obtain the total transmission probability of one monomer  $T_M = |x_j^R|^2$  at  $x_j^L = 1$ ,  $y_j^R = 0$ ,  $kl_{j,A} = \phi_A$  and  $kl_{j,B} = \phi_B$ , which is given by

$$T_M = H^2 / (P^2 + Q^2), \quad (12)$$

where  $H = \sqrt{T}(2\sqrt{R} + \sin 2\phi_A + \sin 2\phi_B)$ ,  $P = 2\sin^2(\phi_A + \phi_B) - \sin^2(\phi_A - \phi_B) + \sqrt{R}(\sin 2\phi_A + \sin 2\phi_B)$ ,  $Q = \sin 2(\phi_A + \phi_B) + \sqrt{R}(\cos 2\phi_A + \cos 2\phi_B)$ . We can find that the resonant tunneling  $T_M = 1$  under the conditions  $\phi_A + \phi_B = \frac{\pi}{2}$  and  $\phi_A = \frac{1}{2} \arcsin(\sqrt{T} - \sqrt{R})$ . In contrast, the classical transmission probability  $T_M^C$  is less than its upper bound  $\frac{3T}{1+2T}$ .

Figure 3(b) shows the total transmission probability of one monomer versus the path phases at  $T=0.01$ . For classical case,  $T_C < 0.029$ , the particle passes through the monomer with very small probability. However, for quantum case, there are eight resonant regions where the particle can pass through the monomer with perfect efficiency. Compared with single pathway, the resonant regions for two pathways become larger and then it is much easier for the exciton absorbed different colors of light to pass through the monomer.

*Transmission of the whole FMO complex.* From Eqs. (6-9), we can obtain the total transmission probability  $T_{FMO} = |O'|^2$  of the whole FMO complex. For simplicity, we assume  $kl_{j,A} + kl_{j,B} = \frac{\pi}{2}$  and the phases accumulated

between  $G$  and  $S$  are an integer of  $2\pi$ . Then we have

$$T_{FMO} = H^2 / Q^2, \quad (13)$$

where  $H = 6\sqrt{T}q_1q_2q_3(3R + 2p_1\sqrt{R} + \frac{1}{2}p_1^2 - \frac{1}{2}p_2)$ ,  $Q = -6p_1R^{\frac{5}{2}} - (11p_1^2 - 6p_2 + 9)R^2 - 2[30p_0 - 7p_3 + p_1(6 + 7p_2)]R^{\frac{3}{2}} - (7p_1^2 + 34p_0p_1 + 4p_2^2 - 3p_2 - 4p_4)R + (9p_0 + 2p_1)(p_2 - p_1^2)R^{\frac{1}{2}} - 9p_0^2 - 2p_1p_0 - \frac{1}{2}p_2^2 + \frac{1}{2}p_4$ . Here  $p_0 = \sin 2\phi_1 \sin 2\phi_2 \sin 2\phi_3$ ,  $p_n = \sin^n 2\phi_1 + \sin^n 2\phi_2 + \sin^n 2\phi_3$  ( $n=1, 2, 3, 4$ ), and  $q_j = \sin 2\phi_j + \sqrt{R}$  with  $\phi_j = kl_{j,A}$ . It is found that the exciton can resonantly pass through FMO when  $\phi_1 = \phi_2 = \phi_3 = \frac{1}{2} \arcsin(\sqrt{T} - \sqrt{R})$ . In contrast, the total classical transmission probability  $T_{FMO}^C$  is less than its upper bound  $\frac{9T}{1+8T}$ . Figure 3(c) shows the quantum transmission of the whole FMO complex for fixing  $\phi_3 = \frac{1}{2} \arcsin(\sqrt{0.12T} - \sqrt{R})$  and  $T=0.01$ . Compared with the transmission of double pathways shown in Fig. 3(b), the resonant region of the whole FMO becomes larger. However, the transmission  $T_{FMO}^C < 0.083$  for classical case, which is pretty small.

Before ending, we make several remarks on the main results that can be obtained from the scattering model: (i) The mechanism underlying the perfect energy efficiency is the resonant transmission induced by the quantum coherent effects, which is impossible for the classical mechanism. (ii) Multi-pathway plays significant role in achieving remarkable efficiency of the energy transfer. To understand this point, we plot in Fig. 3(d) the transmission coefficients for one, two, and multiple pathways. The resonant regions for FMO with multiple pathways almost occupy all parameter space which ensures that the exciton can pass through FMO with perfect efficiency. The large resonant region means that the exciton absorbed different colors of light can still pass through FMO with high efficiency. (iii) The resonant conditions are determined by the space distribution of the pigments. When the pigments are optimally spaced such that the quantum resonant tunneling will happen, the exciton can pass through FMO with perfect efficiency. Therefore, our results prove the conjecture that quantum coherence might 'wire' together the final energy acceptors in antennas, thus compensating for the relatively weak coupling between the pigments in FMO [2, 8]. In addition, FMO with multiple pathways has fault-tolerant function. When one pathway or one subunit is blocked, the exciton can still pass through other pathways.

In summary, we have proposed a scattering model to compare the quantum and classical energy transfer in FMO. We found that, the aforementioned three factors, the optimal space distribution of the pigments, multiple pathways, and quantum effects are combined together to ensure high efficiency of the energy transfer in FMO.

This work was supported by the NNSFC (Nos.11175067, and 11125417), the NBRPC (No.2011CBA00302), the SKPBRC (No.2011CB922104), and the NSF of Guangdong (No.S2011010003323).

---

\* shilzhu@yahoo.com.cn

- [1] R. E. Blankenship, *Molecular Mechanisms of Photosynthesis* (Blackwell Science, Oxford, 2002).
- [2] R. V. Grondelle and V. I. Novoderezhkin, *Nature (London)* **463**, 614 (2010).
- [3] R. V. Grondelle, J. P. Dekker, T. Gillbro, and V. Sundstrom, *Biochim. Biophys. Acta* **1187**, 1 (1994).
- [4] M. K. Sener, J. D. Olsen, C. N. Hunter, and K. Schulten, *Proc. Natl. Acad. Sci. USA* **104**, 15723 (2007).
- [5] G. S. Engel, T. R. Calhoun, E. L. Read, T. K. Ahn, T. Manal, Y. C. Cheng, R. E. Blankenship, and G. R. Fleming, *Nature (London)* **446**, 782 (2007).
- [6] H. Lee, Y. C. Cheng, and G. R. Fleming, *Science* **316**, 1462 (2007).
- [7] G. Panitchayangkoona, D. Hayesa, K. A. Fransteda, J. R. Carama, E. Harela, J. Wenb, R. E. Blankenshipb, and G. S. Engel, *Proc. Natl. Acad. Sci. USA* **107**, 12766 (2010).
- [8] E. Collini, C. Y. Wong, K. E. Wilk, P. M. G. Curmi, P. Brumer, and G. D. Scholes, *Nature (London)* **463**, 644 (2010).
- [9] M. Sarovar, A. Ishizaki, G. R. Fleming, and K. Birgitta Whaley, *Nature Physics* **6**, 462 (2010); A. Ishizaki and G. R. Fleming, *Proc. Natl. Acad. Sci. USA* **106**, 17255(2009).
- [10] S. Yang, D. Z. Xu, Z. Song, and C. P. Sun, *J. Chem. Phys.* **132**, 234501 (2010).
- [11] T. Brixner, J. Stenger, H. M. Vaswani, M. Cho, R. E. Blankenship, and G. R. Fleming, *Nature (London)* **434**, 625 (2005).
- [12] S. Hoyer, M. Sarovar, and K. B. Whaley, *New. J. Phys.* **12**, 065041 (2010); A. Nazir, *Phys. Rev. Lett.* **103**, 146404 (2009); A. Olaya-Castro, C. F. Lee, F. F. Olsen, and N. F. Johnson, *Phys. Rev. B* **78**, 085115 (2008).
- [13] M. Buttiker, Y. Imry, and M. Ya. Azbel, *Phys. Rev. A* **30**, 1982 (1984); Y. Gefen, Y. Imry, and M. Ya. Azbel, *Phys. Rev. Lett.* **52**, 129 (1984).
- [14] S. L. Zhu, D. W. Zhang, and Z. D. Wang, *Phys. Rev. Lett.* **102**, 210403 (2009); S. L. Zhu, and Z. D. Wang, *Phys. Rev. Lett.* **85**, 1076 (2000).